Characterising low-speed, transitional cavity flow

Y. T. Ng
yowthye@stengg.com
Advanced System Department
Singapore Technologies Aerospace Ltd
Singapore

INTRODUCTION

In various studies involving subsonic transition cavity flows, terms like 'transitional-open' and 'transitional-closed' cavity flow regimes are used in the literature. However, the exact fluid dynamic criteria to distinguish them have not been firmly established. The present work attempts to clarify this. Experiments to measure static pressure and fluctuating pressure distribution in a rectangular cavity with length-to-depth (L/D) ratio of 3 to 20 were performed. Based on pressure measurements on the front, bottom and rear faces of the cavity, additional criteria are established to clearly distinguish the range of critical L/D (or $(L/D)_{cri}$) where these different transitional cavity flow regimes occur. The present work ascertains that the $(L/D)_{cri}$ for open and transitional-open cavity flow is 6·0-6·5, for transitional-open and transitional-closed cavity flow is 9-10 and for transitional-closed and closed cavity flow is 14-15. Flow visualisation qualitatively supports the flow pattern in the different cavity flow regimes.

NOMENCLATURE

A_i	pressure amplitude ratio at ith Fourier component
C_p	mean surface pressure coefficient
C_p'	fluctuating surface pressure coefficient
D	cavity depth, m
L	cavity length, m
L/D	length-to-depth ratio
$(L/D)_{cri}$	critical length-to-depth ratio
p_∞	wall surface reference static pressure

Paper No. 3732. Manuscript received 22 June 2011, revised version received 12 December 2011, accepted 12 January 2012.
https://doi.org/10.1017/S0001924000007557 Published online by Cambridge University Press

Re	Reynolds number based on D
U_∞	free stream velocity, ms^{-1}
x	streamwise distance, m
y	depth-wise distance, m
δ_0	boundary-layer thickness corresponding to 99 percent of U_∞
$\Delta\gamma_i$	pressure signal phase shift at i^{th} Fourier component
ρ	density of air, kg/m^3
μ	dynamic viscosity of air, kg/m s

1.0 INTRODUCTION

The presence of a cavity on aerodynamic surfaces can generate unsteady disturbances in the surrounding flow field. Such unsteady cavity flows are known to cause acoustic, vibration and aerodynamic problems. For example, in the wheel wells in the undercarriage of an aircraft, high-intensity acoustic tones can develop and induce vibrations in the surrounding structure, leading to structural fatigue. In addition, for bomb or missile bays (shallow cavity) an adverse static pressure gradient in the cavity can cause the separating store to experience large nose-into-cavity pitching moments thus preventing safe store separation.

Due to its practical applications, cavity flows at different speed regimes have attracted interest among researchers. The early work by Roshko[1] on subsonic cavity flow showed that the interaction between a vortex within the cavity and the separated shear layer causes the latter to deflect into the cavity near its trailing edge and create a high unsteady pressure on the cavity wall. The interaction of the shear layer with the trailing edge is important in the pressure oscillations and sound production by cavities in both low and high speed flows. Rossiter[2], using flow visualisation, showed that vortices in the separated shear layer impinges on the trailing-edge of the cavity and subsequently proposed an empirical relation (the Rossiter equation) to predict the frequency of the periodic pressure fluctuations for different cavity length and Mach number (subsonic and up to M = 1·2). The impingement of vortices on the trailing-edge results in pressure wave propagated upstream in the cavity and when the pressure wave strikes the front face of the cavity, new vortices are formed from the leading edge thus completing a feedback loop. The Rossiter equation was later improved upon by Heller *et al*[3] for higher Mach number flows of 2 to 3. For low-speed cavity flows, measurement of sound production was performed by Yu[4], who made a series of measurement in far-field sound pressure level, fluctuating surface pressure and drag coefficient for shallow and deep cavities. He proposed that the sound radiation from shallow cavity can be modeled by a dipole located at the downstream trailing edge. A review on cavity flow was presented by Rockwell and Naudascher[5].

More recent experimental studies[6,7,8,9] into the vortical structures of low-speed cavity flow were made. An improved understanding of the vortical structures may lead to better techniques to attenuate flow oscillation in low-speed cavity flow. Examples include Ashcroft and Zhang[10] and Özsoy *et al*[11] who both used PIV in the investigation. The former examined the time-averaged vorticity growth rates in the shear layer with downstream distance and found that it is independent of cavity geometry and flow speed. The latter used probability density functions to characterise the vortex location, size and circulation in a cavity. Pereira and Sousa[12] conducted flow visualisation and LDA measurements for subsonic cavity flow and studied the influence of trailing-edge geometry on unsteady cavity flow. Using a sharp, rounded and protruding nose-shaped trailing edge, they found that the cavity with nose-shaped trailing edge was effective in reducing the vertical velocity amplitude. From flow visualisation, this was attributed to the frequent escape of shear layer

https://doi.org/10.1017/S0001924000007557 Published online by Cambridge University Press

vortices before impinging on the trailing edge. A review of the various flow control strategies to attenuate cavity oscillation was provided by Rowley and Williams[13].

Denoting L as the stream-wise cavity length and D its depth, cavity flows are classified as open, transitional, or closed type for different length-to-depth (L/D) ratio. Plentovich *et al*[14] characterised the flow at subsonic and transonic speeds (M = 0·2 to 1·2) while Stallings and Wilcox[15] studied it at supersonic speeds (M = 1·5 and 2·86). Both investigations used the cavity's surface pressure (C_p) distribution to differentiate the various flow types. The L/D ratio for each flow type is also dependent on the flow regime. For subsonic flows, the open cavity flow regime takes place when $L/D < 6$. The shear layer spans the cavity length and reattaches at or downstream of the trailing edge. The surface pressure distribution in the cavity is concave upwards. With L/D at 6 to 8 and beyond, the flow enters the transitional cavity flow regime. The unsteady shear layer flaps and impinges onto the rear face of the cavity and possibly on the aft portion of the cavity floor. This flow type has a concave downward surface pressure distribution on the cavity floor. Finally, with L/D at 12 to 15 and beyond, closed-type cavity flow is observed. For closed cavity flows, the shear layer separates at the cavity leading edge, reattaches on the cavity floor and separates ahead of the rear face. Typical surface pressure distribution on the cavity floor shows a distinct inflection point due to the shear layer reattachment and its subsequent separation. Due to the reattachment of the shear layer on the cavity floor, the fluctuating C_P (or C_P') distribution within the cavity has a local maximum.

The above mentioned 'markers' to identify the critical L/D for different cavity flow types are well documented for subsonic flow. However, recent studies have made more detailed divisions in transitional cavity flow into transitional-open and transitional-closed type. The critical L/D and their criteria where these flow types occur in subsonic flow are not well documented especially for low-speed cavity flows. The objective of this study is to present a set of criteria for each flow type and the critical L/D at which these transitions occur, especially that between transitional-open and transitional-closed. These criteria are also based on mean and fluctuating C_P measured on the front wall, bottom wall and rear wall of the cavity and are limited to a flow speed of U_∞ = 10ms^{-1} (Re = 3·16 × 10^4) with a cavity L/D = 3 to 20. In the next section, the experimental set-up is described.

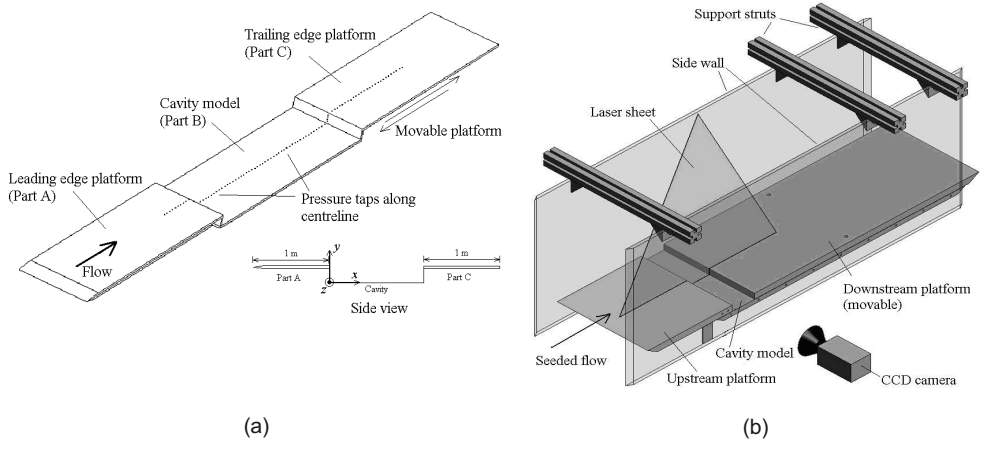


Figure 1. (a) Experimental set-up in a wind tunnel for pressure measurements, (b) Experimental set-up in a water tunnel for flow visualisation.

https://doi.org/10.1017/S0001924000007557 Published online by Cambridge University Press

2.0 EXPERIMENTAL SET-UP

2.1 Wind tunnel and cavity model

The experiments were conducted in a subsonic, open loop suction-type wind tunnel. The internal dimensions of the test section measured 0·342m by 0·342m. The flow velocity $U_\infty = 10\text{ms}^{-1}$, giving a Reynolds number (Re) based on cavity depth ($D = 0{\cdot}05$m) of $3{\cdot}16 \times 10^4$. Fig. 1(a) shows a picture of the cavity model and the co-ordinate system, with the origin located on mid span and on the floor of the cavity. The x-axis points downstream and the y-axis points vertically upwards. The model set-up consist of an upstream leading edge platform (Part A with length = 1m), the rectangular cavity model (Part B) in the middle and a downstream rear platform (Part C, length = 1m). The overall length of the cavity (L) was varied by translating the rear platform of Part C in the x-direction, thus giving any L/D value of 3 to 20. This range of L/D ratio covers the open to closed cavity flow regime.

A total of 98 pressure taps were located along the mid span (or center line) of the cavity model. 10 pressure taps were located on the upstream platform, 4 on the front face of the cavity, 50 on the bottom face, 4 on the rear face and 30 on the downstream platform. The location of these pressure taps are shown in Fig. 1(a). All pressure taps were connected to Scanivalve pressure scanner via PVC tubes of 1·8mm internal diameter. Data was acquired at 10kHz for 131,072 samples to avoid aliasing. All data was acquired and stored in a computer via an analog-to-digital card. The reference static pressure, p_∞, was measured at $10D$ upstream from the step face, on the side wall of the wind tunnel. This was to ensure that the static pressure measured would be free of any effects caused by the step. The error in velocity measurement is 0·5% and the error in pressure coefficient is 2%.

2.2 Fluctuating pressure measurement

It is well known that pressure signals measured using long tubings experience signal attenuation and phase shift due to the inertia of the air in the tubing. The tubing's frequency response was calibrated before the experiment so that the signal's amplitude and frequency can be subsequently corrected and this method was based on the work by Luo and Gan[16]. Essentially, a fluctuating pressure signal of known frequency and amplitude was fed into both long (210mm) and short tubing (30mm), with the time-varying output of both tubings measured and digitally recorded. It was assumed that the pressure output from the short tubing did not experience signal attenuation or phase shift and it was used as the reference pressure signal. Fast Fourier Transform (FFT) was then applied to both signals to obtain the amplitude and phase of each Fourier components. Defining A_i as the ratio of pressure amplitude of the long tubing to short tubing and $\Delta_{\gamma i}$ as the phase shift between the pressure signal of the long and short tubing at the ith Fourier component, the magnitude and phase of each Fourier component from the long tubing's signal is corrected using A_i and $\Delta_{\gamma i}$. The corrected Fourier series representation was inversed transformed (Inverse Fourier Transform) to form the corrected pressure signal from which mean and fluctuating pressure coefficient was computed.

Due to the low-speed nature of the present work, acoustic resonance is not expected to be a dominant feature except for cavities of low L/D of less than 4. Evidence from published works illustrates this. For example, Ashcroft and Zhang[10] detected weak tonal pressure components in the spectra for a cavity with $L/D = 4$ and at different flow speeds of 32, 37 and 42ms^{-1}. This corresponds to Re = $1{\cdot}1 \times 10^5$, $1{\cdot}3 \times 10^5$ and $1{\cdot}4 \times 10^5$. These weak tonal pressure fluctuations

https://doi.org/10.1017/S0001924000007557 Published online by Cambridge University Press

correspond to the Rossiter modes. They point to low L/D between 2 to 4 where the weak modes are more distinct. Pressure fluctuations are more distinct at lower L/D and this point was shown in the work of Ukeiley and Murray[6]. The flow speed was 68ms^{-1} and they showed that for cavities with L/D = 1·49 to 5·16, flow resonance (as detected from pressure spectra) was detected in the low L/D = 1·49, 1·92, 2·375 and 2·38 but not at higher L/D = 5·16. The pressure spectra from their work showed the presence of two distinct frequencies, which correspond well to the two Rossiter modes. Finally at an even lower L/D = 1, Chatellier *et al*[7] detected 4 frequency bands (or modes) at speeds of 29, 31 and 36ms^{-1}. These 4 frequency bands were traced to hydrodynamic fluctuations and aero-acoustic coupling. At such low L/D, the fluctuations were predominantly acoustic modes similar to those found in open resonators. The work by Grace *et al*[8] for a cavity of L/D = 4 and at flow speeds of 7·5ms^{-1} and 15ms^{-1} also did not detect cavity resonance.

From the discussion above, it indicates that acoustic resonance is dominant at low L/D (less than 4) for low subsonic flow. As the present work involves cavities of large L/D, and for consistency throughout the paper, pressure spectral data is not presented for the low L/D cases.

2.3 Experimental flow visualisation

The flow over a cavity was visualised in a re-circulating water channel. The cross section of the water channel measured 0·4m by 0·4m and Fig. 1(b) shows the experimental set-up. Similar to the wind-tunnel experiment, the cavity model used in flow visualisation consist of three parts, namely the upstream platform, the cavity model and a downstream platform. The cavity depth was D = 0·02m and the overall cavity length, L, could be varied by translating the downstream platform. The range of L/D was 3 to 20 at discrete interval of 1D. The water channel was uniformly seeded with 60μm particles and illuminated with a continuous laser sheet which was aligned along the mid-span of the cavity model. The flow velocity in the water channel was 0·15ms^{-1}, giving a Re = 2,989 (based on cavity depth). A CCD (coupled-charged device) camera was focused on the illuminated particles on the laser sheet. By opening the camera shutter for an extended period of time ($\Delta t \approx 0{\cdot}2$ sec), short pathlines of the particles in the flow field can be imaged and flow structures visualised. Both video and still pictures were taken in this experiment.

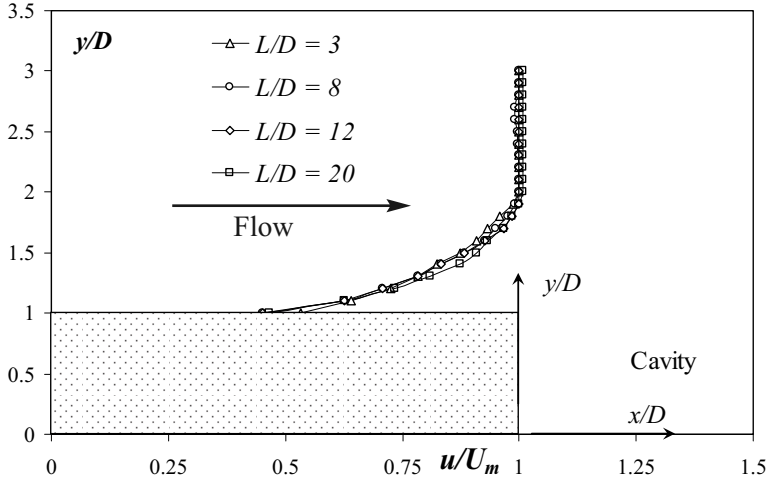


Figure 2. Velocity and boundary-layer profiles upstream of the cavity at different L/D ratios.

https://doi.org/10.1017/S0001924000007557 Published online by Cambridge University Press

Although the flow velocity and Re in the visualisation study was considerably lower than that conducted in the wind tunnel, the purpose of conducting the flow visualisation in water was simply to illustrate qualitatively some of the flow features that one should expect to see in different cavity flow regimes. These visualised structures highlight the salient feature of each flow regime only and not used to determine the critical L/D for each cavity transition regimes.

2.4 Boundary-Layer measurement

The boundary layer was measured upstream of the cavity at $x/D = -2{\cdot}0$ using a Pitot-static tube in the wind tunnel. It was measured for four different cavity $L/D = 3$, 8, 12 and 20. The boundary-layer profiles are shown in Fig. 2 and for clarity, an outline of the cavity's leading edge platform is also shown in the same figure. The boundary-layer profiles and boundary-layer thicknesses remain relatively uniform for cavities of different L/D ratios although a small increase in speed is noted for the largest $L/D = 20$. For such cavities, the trajectory of the shear layer bends into the cavity after separating from the leading edge. The noted variation could be attributed to localised flow acceleration as the shear layer bends into the cavity. In this experiment, the averaged boundary-layer thickness was $\delta_0 = 43{\cdot}5$mm (or $\delta_0 = 0{\cdot}87D$).

2.5 Three dimensional effects

The three-dimensional flow structure in the cavity was assessed by conducting tuft flow visualisation at selected $L/D = 3$, 8 13 and 20 in the wind tunnel at $U_m = 10\text{ms}^{-1}$. The objective was to provide a preliminary insight of the three dimensional flow structures and the extent of their influence. For low $L/D = 3$ to 8, the tufts were noted to flap energetically and randomly in the re-circulating flow regions and near walls. Three dimensional flows were localised within these regions and this was assessed visually by noting that the tufts were generally not aligned in the stream-wise direction. With increase in L/D to 13 and 20, the shear layer reattached onto the cavity floor, the tufts were aligned with the stream-wise flow and were relatively stationary (not flapping). The flow is generally two dimensional in these regions.

The tuft flow visualisation revealed that localised three dimensional flow structures and possibly vortical flow exist in the cavity particularly near walls. In the present work, a central line pressure measurement was adopted in wind-tunnel experiment to correlate the data with the flow structures found in the single laser sheet flow visualisation conducted in the water tunnel. Published literature usually report pressure measurements and flow visualisation on the mid-span of the cavity to distinguish the different flow regimes. To present the pressure data in a consistent manner, the

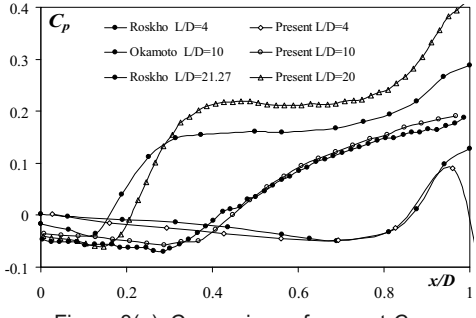


Figure 3(a). Comparison of present C_p results derived from cavity flow with those of Roshko[1] and Okamoto *et al*[17].

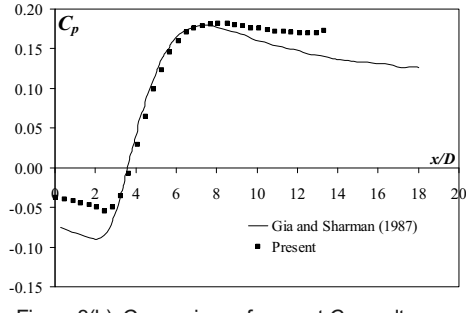


Figure 3(b). Comparison of present C_p results derived from the flow over a backward facing step with those of Gai and Sharman[18].

https://doi.org/10.1017/S0001924000007557 Published online by Cambridge University Press

present experiment adopted the same approach by using a single mid-line pressure survey instead of reporting on the details of corner vortices or three-dimensionality.

In the next section, the experimental results are benchmarked with those in published literature. The C_P measurements are presented and the criteria to define the critical (L/D) ratio for each flow regime are stated.

3.0 RESULTS AND DISCUSSION

3.1 Comparative study

To benchmark the experimental results and technique, the C_P distribution is compared with those of Roshko[1] and Okamoto *et al*[17] on a flow past a cavity and those of Gai and Sharma[18] on the flow over a backward facing step. The comparative study was limited to low subsonic flow. In Roshko's[1] work, the flow velocity was 23ms^{-1} (or 75ft/s) and the cavity depth could be varied from 0 to 10 inches (i.e. up to 254mm). The cavity's span-wise and stream-wise dimensions were kept fixed at 4 inches and 32 inches (or 101·6mm and 812mm) respectively. At L/D = 21·3 (as shown in Fig. 3(a)), the Re based on cavity depth of 1·5 inches (or 38·1mm) was $5{\cdot}54 \times 10^4$, which is comparable to the Re = $3{\cdot}16 \times 10^4$ of this study. In Okamoto *et al*'s[17] work, the Re = $1{\cdot}04 \times 10^4$ at a flow velocity of 5ms^{-1} and cavity depth of 30mm. The Re in their work is also comparable to the present study.

The C_P distribution from the cavity of L/D = 4 and 20 are compared against those of Roshko's[1] cavity of L/D = 4 and 21·27 respectively, and the L/D = 10 with that from Okamoto *et al*[17]. To make comparison with Gai and Sharman[17], the downstream rear platform (Part C) was removed so that the experimental rig was a backward facing step. Fig. 3(a) and (b) show the comparative study respectively.

From Fig. 3(a), the data agrees reasonably well with Roshko's[1] and Okamoto *et al*'s[17] data, especially at lower L/D ratios. In addition, both studies predicted that at L/D = 4, the flow is in the open cavity flow regime (due to a concave upward trend in C_p), at L/D = 10, the flow is in the transitional flow regime (due to the concave downward trend in C_p), and at L/D = 20, the flow is in the closed cavity flow regime (due to the presence of an inflection point in the C_p trend). However, for the larger L/D = 20, there is a greater observed discrepancy (about 20%), which can be explained as follows. Roshko[1] used a cavity that was four inches long and varied the cavity depth (D), instead of the length (L) to achieve different L/D ratios. He stated the boundary-layer thickness was about δ = 25mm in his experiment while for the current experiment, the boundary layer is about δ = 43·5mm thick. Therefore, the ratio of δ/D was variable in Roshko's[1] experiment due to the changing depth of his apparatus while it is kept relatively constant (at δ/D = 0·87) in this experiment.

From Fig. 3(b), the comparison with Gai and Sharman[18] on the backward facing step shows fair agreement. The reattachment position, corresponding to the position of the maximum C_P value, was estimated to be about x/D = 6·8 and at a maximum C_P value of 0·18. This is in good agreement with data from the reference, where the reattachment region was in the region of x/D = 6 to 7, and a maximum C_P value of 0·17.

The experimental results compare fairly well with those from the literature and in the next section, the various criteria for the determination of $(L/D)_{cri}$ for the different low-speed cavity flow transition regimes are described.

https://doi.org/10.1017/S0001924000007557 Published online by Cambridge University Press

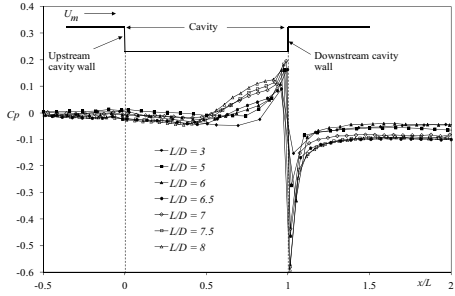


Figure 4(a). Overall C_p distribution for cavity with L/D of 3 to 8 in the open and transitional-open flow regime.

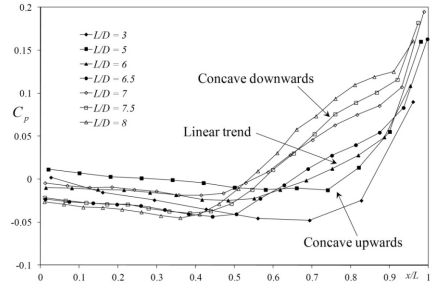


Figure 4(b). Detailed C_p distribution on the bottom floor of a cavity with L/D of 3 to 8 in the open and transitional-open flow regime.

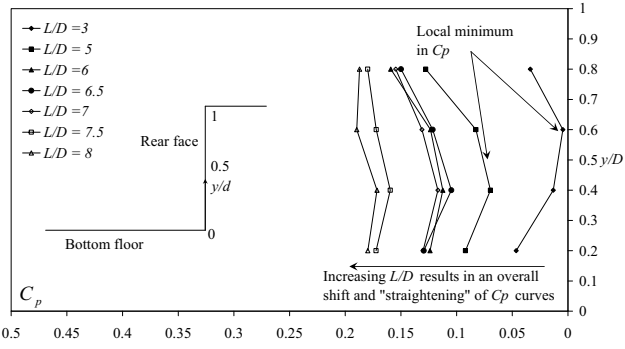


Figure 5. C_p distribution on the rear face of a cavity with L/D of 3 to 8. Increasing L/D leads to an overall shift and straightening of the C_p curves.

3.2 Open and transitional-open cavity flows

Fig. 4(a) shows the entire surface C_P distribution obtained for cavity L/D of 3 to 8 while Fig. 4(b) shows the same but a more detailed C_P distribution for the cavity's bottom floor. To aid understanding, an outline of the cavity is included in Fig. 4(a). The range of L/D covers the open and transitional-open cavity flow regime and the objective is to propose an 'indicator' that marks the $(L/D)_{cri}$ where a change of flow regime takes place. As shown in Fig. 4(a), the C_P upstream of the cavity is slightly negative but relatively uniform, and becomes more negative as it approaches the leading edge of the cavity. On the floor of the cavity, the C_P values continue to decrease, before increasing in the aft portion of the cavity near the rear face. In Fig. 4(b), the detailed plot of C_P distribution on the cavity floor clearly shows the characteristic concave-up C_P distribution for cavity of L/D = 3-6, indicating open cavity flow. With a slight increase of L/D to 6·5, the C_P distribution on the floor of the cavity (Fig. 4(b)) changes from a concave up to an almost linear trend at L/D = 6·5. Beyond L/D = 6·5, the C_P distribution show that it changes into a concave-downward trend. It is generally accepted that a concave-downward trend in the C_P distribution indicates transitional cavity flow and the above finding provides a suitable 'indicator' for the $(L/D)_{cri}$ at which open and transitional-open cavity flow take place. The experimental results, therefore, shows that it occurs at $(L/D)_{cri}$ = 6·5 and when the C_P distribution on the floor of the cavity presents a generally linear trend.

To provide additional 'indicators' for the $(L/D)_{cri}$ at which open and transitional-open cavity flow take place, it is of interest to study the C_P distribution on the rear face of the cavity in the range

https://doi.org/10.1017/S0001924000007557 Published online by Cambridge University Press

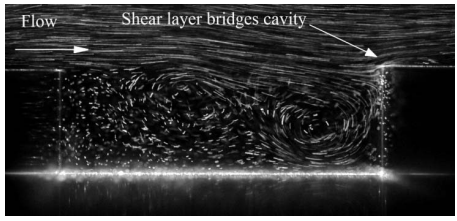


Figure 6(a). Particle flow visualisation showing the shear layer bridges the cavity. A feature of open cavity flow.

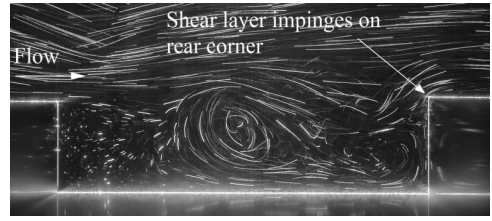


Figure 6(b). Particle flow visualisation showing the shear layer impinges on rear face and corner. Transitional-open cavity flow.

of $L/D = 3$ to 8 and this is shown in Fig. 5. The horizontal C_P axis in Fig. 5 is plotted with increasing magnitude to the left and the vertical y/D axis denotes the vertical height on the rear face. For clarity, an outline of the cavity rear face is also shown. The figure shows that at small $L/D = 3$, the C_P distribution shows a minimum (or low pressure) at mid-height of the rear face. As L/D increases, the C_P along the rear face increases, as denoted by the overall shift in the curves to the left. In addition, the C_P distribution shows increased uniformity on the rear face as depicted by the 'straightening' of these curves. These results are not surprising as this trend can be traced to the changes in shear layer impinging onto different locations near the rear corner (or rear face) when L/D increases from open cavity to transitional cavity flows. It can be argued that, with a larger L/D, the time-averaged trajectory of the shear layer impinges onto a lower (lesser y/D) portion of the rear face, thus increasing the side wall pressure and the magnitude of C_P and hence a more uniform distribution.

The flow visualisation indicates clearly the flow structures discussed above for an open and transitional-open cavity flow and this is illustrated in Fig. 6(a) and (b) respectively. Flow visualisation in Fig. 6(a) shows that for an open cavity flow, the shear layer bridges across the cavity and a captive vortex is present in the cavity as shown. This vortex is located near the downstream half of the cavity and it was observed during flow visualisation that both the shear layer and the vortex are unsteady. The shear layer is noted to flap (though not periodically) and the formation of the vortex depends on fluid being fed from the shear layer. In some instances, the vortex in the cavity dissipates abruptly (or breaks up), most probably due to fluid vented out of the cavity when the shear layer is on the upstroke. With an increase of L/D to the transitional-open cavity flow regime, there is increased unsteadiness in the shear layer and in the vortical structures in the cavity. Due to the larger L/D, the shear layer may not bridge the cavity completely and is noted to impinge onto the rear face intermittently. This is shown and labeled in Fig. 6(b). The intermittent shear layer

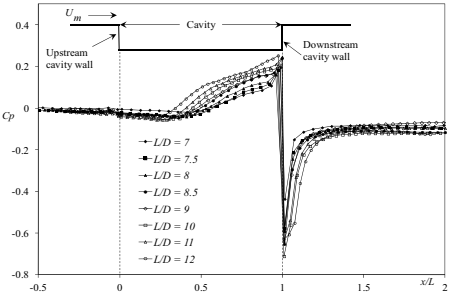


Figure 7(a). Overall C_p distribution for cavity L/D of 7 to 12 in the transitional open and transitional-closed flow regime.

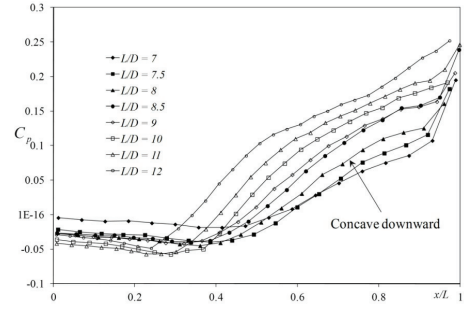


Figure 7(b). Detailed C_p distribution on the bottom floor of a cavity with L/D of 7 to 12 in the transitional-open and transitional-closed flow regime.

https://doi.org/10.1017/S0001924000007557 Published online by Cambridge University Press

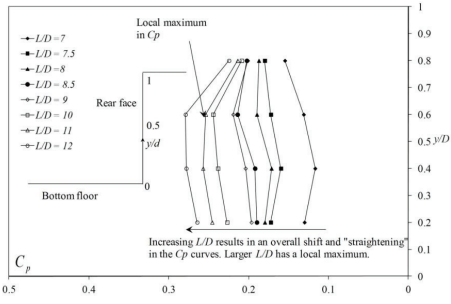


Figure 8(a). C_p distribution on the rear face of a cavity for L/D of 7 to 12. Increasing L/D leads to an overall shift and straightening of the C_p curves. For larger L/D, a local maximum is noted.

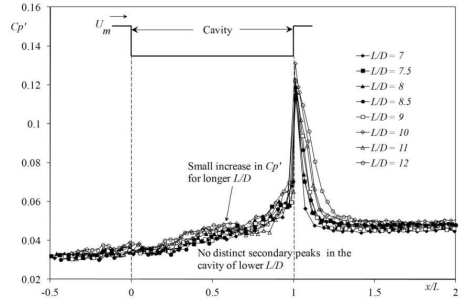


Figure 8(b). C_p' distribution for cavity with L/D ratio of 7 to 12. Maximum C_p' is noted at the rear corner of the cavity.

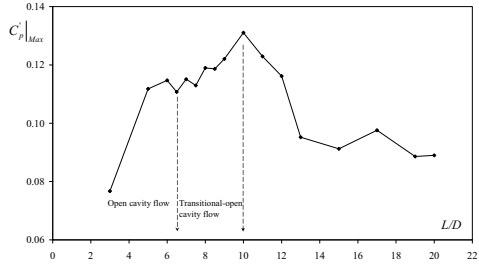


Figure 9. Variation of $C_p'|_{max}$ with L/D. A local maximum in $C_p'|_{max}$ is noted at L/D = 10, which indicates the end of the transitional-open cavity flow regime.

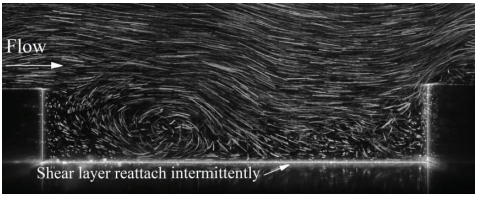


Figure 10. Particle flow visualisation showing the shear layer impinges deeper into the cavity and rear face. Transitional-closed cavity flow.

impingement onto the rear face alters the C_P distribution on that face from one with a local minimum to one which is relatively uniform. This was discussed previously with the aid of Fig. 5. Shear layer impingement onto the rear face occurs in the transitional-open and transitional-closed regime. Using this knowledge, another criterion is proposed in the next section to indicate the $(L/D)_{cri}$ at which these transitions occur.

3.3 Transitional-open and transitional-closed cavity flows

Figure 7(a) shows the overall C_P distribution obtained for the cavity L/D of 7 to 12 while Fig. 7(b) shows a detailed plot of the C_P distribution on the bottom wall of the cavity measured for the same L/D. The C_P distribution shows an increased concave-downward trend with L/D in the transitional cavity flow regime. In this regime, the flow is characterised with increased (or more energetic) fluctuations and is coupled with impingement of the shear layer onto the cavity's rear face. With this knowledge, the averaged C_P distribution on the cavity's bottom floor may not reveal the criteria necessary to mark the change between transitional-open and transitional-closed cavity flow. A better set of indicators may lie in the averaged C_P distribution on the cavity's rear wall and the overall distribution of fluctuating C_P (or C_P'). This is shown, respectively, in Fig. 8(a) and (b) for L/D = 7 to 12. In Fig. 8(a), and with increasing L/D of 7 to approximately 9, the C_P distribution on the rear face becomes relatively more uniform. At L/D = 8·5-9, the C_P distribution presents a relatively linear trend and with further increase in L/D of 10 to 12, the C_P distribution exhibits a distinct local maximum at around the mid-height of the rear face. Since the variation of the C_P distribution on

https://doi.org/10.1017/S0001924000007557 Published online by Cambridge University Press

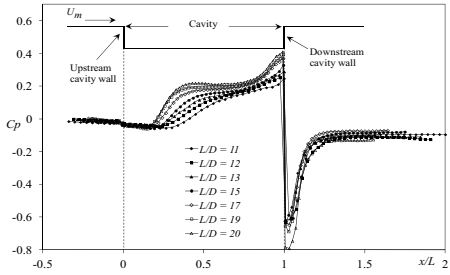


Figure 11(a). Overall C_p distribution for cavity L/D of 11 to 20 in the transitional-closed and closed cavity flow regime.

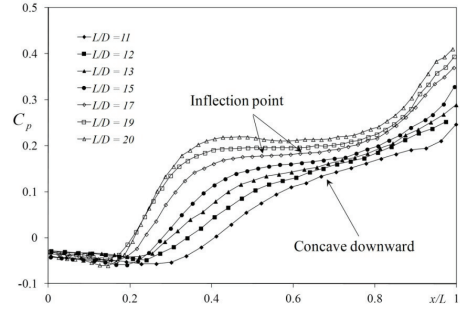


Figure 11(b). Detailed C_p distribution on the bottom floor of a cavity with L/D of 11 to 20 in the transitional-closed and closed flow regime. Presence of inflection point indicates closed cavity flow.

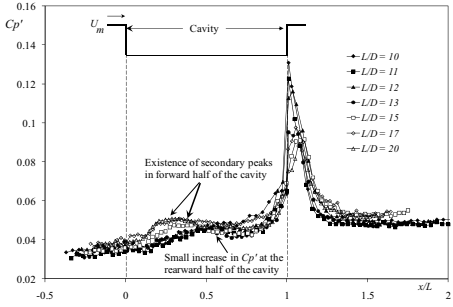


Figure 12. C_p' distribution for cavity with L/D ratio of 10 to 20. Secondary peaks in C_p' are noted at the forward part of the cavity.

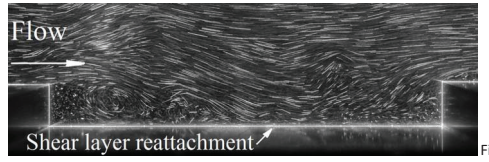


Figure 13. Particle flow visualisation showing the shear layer reattachment on the bottom floor of the cavity. A feature of closed cavity flow.

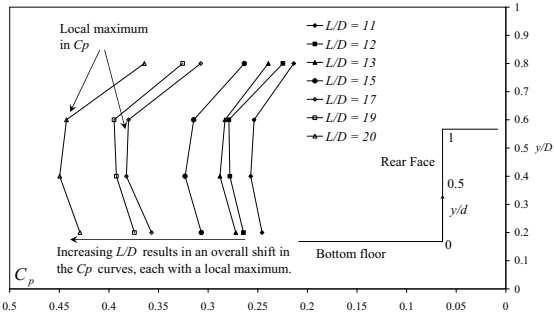
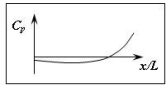
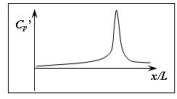
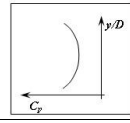
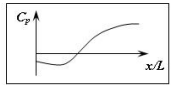
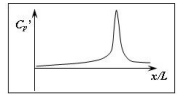
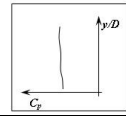
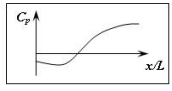
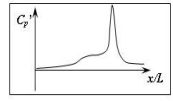
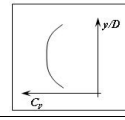
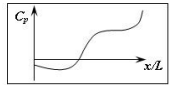
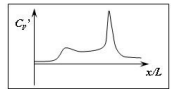
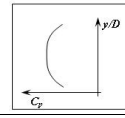


Figure 14. C_p distribution on the rear face of a cavity for L/D of 11 to 20. Increasing L/D leads to an overall shift of the C_p curves, each with a local maximum value.

the rear face changes from one that contains a local minimum to one that contains a local maximum, one can use this as a criterion to mark the critical (L/D) at which the flow changes its character from transitional-open to transitional-closed cavity flow. However, due to the highly unsteady nature in transitional cavity flows, C_p' is used as an additional criteria for this purpose. Fig. 8(b) shows the overall C_P' distribution in the cavity for L/D = 7 to 12 and a distinctive peak exist in the rear corner, thus implying that the shear layer interacts with (or impinges onto) the rear

https://doi.org/10.1017/S0001924000007557 Published online by Cambridge University Press

Table 1
Summary for different types of cavity flow regime and their respective C_p and C_p' characteristics

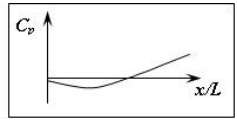
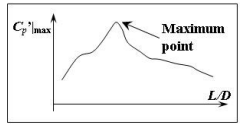
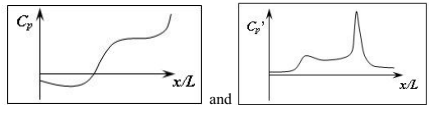
	Criteria for flow regime		
	Shape of C_p curve	Shape of C_p' curve	Shape of C_p curve over the rear face
Open cavity flow regime. ($L/D < 6.5$)	Concave up in the aft portion of the cavity. 	No secondary peaks present. 	With local minimum point. 
Transition-open cavity flow regime. ($6.5 < L/D < 10$)	Concave down in the aft portion of the cavity. 	No secondary peak present. 	Relatively linear in shape. 
Transition-closed cavity flow regime. ($10 < L/D < 15$)	Concave down in the aft portion of the cavity. 	Slight secondary peak present. 	With a local maximum point. 
Closed cavity flow regime. ($L/D > 15$)	Inflection point present. 	Secondary peak present 	With a local maximum point. 

corner resulting in strong pressure fluctuations. Of particular interest is the maximum C_P' (or $C_P'|_{max}$) for each cavity's L/D. By plotting $C_P'|_{max}$ with L/D in Fig. 9, one notes that $C_P'|_{max}$ increases in the open and transitional-open cavity flow regime. $C_P'|_{max}$ reaches a maximum value at $L/D = 10$ and subsequently decreases in magnitude with further increase in L/D. This finding at $L/D = 10$ coincides well with the previous finding that at $L/D = 9$, a fairly linear C_P distribution on the rear face exist. It can be conjectured that the strong pressure fluctuations due to shear layer impingement at the rear corner, led to a fairly linear C_P variation on the rear face of the cavity at L/D = 9-10. Taken together, these two criteria can be used as 'indicators' to mark the transition between transitional-open and transitional-closed cavity flows and the $(L/D)_{cri}$ at which this occurs is L/D = 9-10. Beyond this $(L/D)_{cri}$ implies that the flow is intermediate between the transitional-closed cavity regime and the closed cavity flow regime.

Flow visualisation of Fig. 10 demonstrates the major flow features in transitional-closed cavity flows. The shear layer impinges onto the rear corner and the trajectory of the shear layer near the aft of the cavity curve downwards into the cavity. From the flow visualisation, no firm shear layer reattachment on the bottom floor of the cavity takes place. The shear layer was seen to reattach intermittently on the floor of the cavity. This intermittent reattachment of the shear layer onto the floor of the cavity could explain the absence of an inflection point in the C_P distribution in Fig. 7(b) and presence of a slight raised plateau in the C_P' distribution for longer L/D in Fig. 8(b). This slight increase in C_P' could be a manifestation of the intermittent reattachment of shear layer onto

https://doi.org/10.1017/S0001924000007557 Published online by Cambridge University Press

Table 2
Criteria for C_p and C_p' for the determination of critical (L/D) at different flow transition regimes

Flow Regime	Criteria for C_p and (or) C_p' to determine $(L/D)_{cri}$
Open to Transitional-open cavity flow. $(L/D)_{cri} = 6.5$	C_P distribution is linear in the aft portion of the cavity. 
Transitional-open to Transitional-closed cavity flow. $(L/D)_{cri} = 10$	$C_p'\|_{max}$ reaches a maximum value. 
Transitional-closed to Closed cavity flow. $(L/D)_{cri} = 15$	C_p distribution contains an inflection point and a secondary peak appear in the C_p' distribution. 

the cavity floor. In the next section, the $(L/D)_{cri}$ for transitional-closed and closed cavity will be stated based the presence of an inflection point in the C_P distribution and a distinct secondary peak in the C_P' distribution.

4.0 TRANSITIONAL-CLOSED AND CLOSED CAVITY FLOW

Fig. 11(a) and (b) shows respectively, the overall and detailed C_P distribution on the cavity wall as measured from the experiment for L/D = 11 to 20. Fig. 11(b) clearly shows that as L/D increases, the C_P variation changes from a concave-downward trend to one with an inflection point. This inflection point has a relatively flat plateau at L/D = 15 and it is generally accepted in the literature that a point of inflection in the C_P distribution indicates closed cavity flows. The existence of the point of inflection indicates that the shear layer reattaches onto the cavity floor and subsequently separates at a downstream location and flows over the rear corner. In addition to the C_P distribution, the C_P' is used as another criterion to indicate the $(L/D)_{cri}$ between transitional-closed and closed cavity flow. This is shown in Fig. 12. In the transitional-closed regime of L/D = 11-13, a small increase in C_P' is noted on the downstream half of $x/L > 0{\cdot}5$ before the rear face on the cavity floor. The x/L location at which this small increase in C_P' occurs seems to be unaffected by changes in L/D from 11 to 13. With an increase of L/D = 15 and beyond, a secondary peak in C_P' is observed which is located in the forward half of the cavity floor (that is $0 < x/L < 0{\cdot}5$). This indicates that the shear layer has reattached fully onto the floor of the cavity and an enclosed eddy is present in the forward half of the cavity, thus implying closed cavity flow.

Flow visualisation (as shown in Fig. 13) shows the main features of closed cavity flow. The shear layer that forms after separating from the leading edge has a downward trajectory. It reattaches

https://doi.org/10.1017/S0001924000007557 Published online by Cambridge University Press

onto the floor of the cavity as indicated and separates again at a downstream location. Captive eddies can be observed in the forward half of the cavity.

It is also of interest to study the C_P distribution on the rear faces of the cavity in this flow transition regime which is shown in Fig. 14. The pressure distribution on the rear face shows a local maximum in C_P. In addition, the magnitude of C_P on the rear face increases with L/D.

From the results presented, the initial occurrence of a secondary peak in the C_P' distribution at L/D = 15 and the presence of an inflection point in the C_P distribution can be used as criteria to indicate the $(L/D)_{cri}$ for transitional-closed and closed cavity flows. In this present work, it is at $(L/D)_{cri}$ = 15.

5.0 SUMMARY OF RESULTS

In the discussion provided above, various criterions based on measurements of C_P and C_P' distribution on the cavity walls were stated to indicate the $(L/D)_{cri}$ for open, transitional-open, transitional-closed and closed cavity flows. Table 1 provides a pictorial summary of the different characteristics for C_P and C_P' at each flow regime for low-speed cavity flow (such as the one that was tested). Table 2 illustrates the criteria necessary for determining the critical (L/D) for each flow regime. It is hoped that this summary will be useful to characterise transitional cavity flows and possibly extend the definitions here to other flow speeds and regimes.

6.0 CONCLUSION

From the literature, C_p is the most conventional and widely used quantity for the evaluation and identification of cavity flow characteristics. In this study, C_P' is shown to be a good complement to C_P in identifying the different transitional cavity flow regimes. Based on C_P and C_P' distribution on the walls of a cavity, different criteria were proposed to indicate the critical (L/D) at which different transition regimes occur in cavity flow. Between open and transitional-open cavity flows, the C_P distribution on the floor of the cavity should exhibit a linear variation and the $(L/D)_{cri}$ = 6·5. Between transitional-open and transitional-closed, the C_P distribution on the rear face of the cavity should exhibit a linear trend and the $C_P'|_{max}$ attains a maximum value. This occurs at $(L/D)_{cri}$ = 10. And between transitional-closed and closed cavity flows, an inflection point in the C_p distribution should be present coupled with the existence of a secondary peak in the C_P' distribution. This takes place at $(L/D)_{cri}$ = 14-15. The use of these quantitative indicators provides convenient and clear markers to pin-point the boundaries for each transition flow regime. Flow visualisation was used as a supplementary tool to illustrate qualitatively the different features in the cavity flow regimes. It is hoped that the listed criteria act as a starting platform and can be extended to cavity flows of other flow speeds. Therefore, it should not be surprising that the critical L/D ratio may differ for cavity flows of other Reynolds number (or Mach number).

REFERENCES

1. ROSHKO, A. Some Measurements of Flow in a Rectangular Cutout, NACA Tech Note 3488, August 1955.
2. ROSSITER, J.E. Wind Tunnel Experiment on the Flow over Rectangular Cavities at Subsonic and Transonic Speeds, Reports and Memoranda, 3438, British Aeronautical Research Council, 1966.
3. HELLER, H.H., HOLMES, D.G. and COVERT, E.E. Flow-induced pressure oscillations in shallow cavities, *J Sound and Vibration*, 1971, **18**, 4, pp 545-553.

https://doi.org/10.1017/S0001924000007557 Published online by Cambridge University Press

4. YU, Y.H. Measurement of sound radiation from cavities at subsonic speeds, *J Aircr*, 1977, **14**, (9), pp 838-843.
5. ROCKWELL, D. and NAUDASCHER, E. Review-self sustaining oscillations of flow past cavities, *transactions of the ASME*, June 1978, **100**, pp 152-165.
6. UKEILEY, L. and MURRAY, N. Velocity and surface pressure measurements in an open cavity, *Experiments in Fluids*, 2005, **38**, pp 656-671.
7. CHATELLIER, L., LAUMONIER, J. and GERVAIS, Y. Theoretical and experimental investigations of low Mach number turbulent cavity flows, *Experiments in Fluids*, 2004, **36**, (5), pp 728-740.
8. GRACE, S.M., DEWAR, W.G. and WROBLEWSKI, D.E. Experimental investigation of the flow characteristics within a shallow wall cavity for both laminar and turbulent upstream boundary layers, *Experiments in Fluids*, 2004, **36**, pp 791-804.
9. SAVORY, E., TOY, N., DISIMILE, P.J. and DIMICCO, R.G. The drag of three-dimensional rectangular cavities, *Applied Scientific Research*, May 1993, **50**, 3-4, pp 325-346.
10. ASHCROFT, G. and ZHANG, X. Vortical structures over rectangular cavities at low speed, *Physics of Fluids*, **17**, 015104, 2005.
11. ÖZSOY, E., RAMBAUD, P., STITOU, A. and RIETHMULLER, M.L. Vortex characteristics in laminar cavity flow at very low Mach number, *Experiments in Fluids*, 2005, **38**, pp 133-145.
12. PEREIRA, J.C.F. and SOUSA, J.M.M. Influence of impingement edge geometry on cavity flow oscillations, *AIAA J*, 1994, **32**, (8), pp 1737-1740.
13. ROWLEY, C.W. and WILLIAMS, D.R. Dynamics and control of high Reynolds number flow over open cavities, *Annual Review of Fluid Mechanics*, 2006, **38**, pp 251-276.
14. PLENTOVICH, E. B., STALLINGS, R.L. JR and TRACY, M.B. Experimental Cavity Pressure Measurements at Subsonic and Transonic Speeds: Static-Pressure Results, NASA Technical Paper 3358, December 1993, p 80.
15. STALLINGS, R.L. JR and WILCOX, F.J. Jr Experimental Cavity Pressure Distributions at Supersonic Speeds, NASA Technical Paper 2683, June 1987, p 77.
16 Luo, S.C. and GAN, T.L. Correction of distortion in fluctuating pressure signal caused by long pressure transmitting PVC tubing, *J Institute of Engineers Singapore*, 1991, **31**, pp 33-35.
17 OKAMOTO, S., MISUTANI, Y. and YAMASAKI, T. Flow in Two-dimensional Rectangular Cavities, *Transactions of the Japan Society of Mechanical Engineers*, *Part B*, February 2002, **68**, 666, pp 384-392 (in Japanese).
18. GAI, S.L. and SHARMA, S.D. Pressure Distributions behind a Rearward Facing Segmented Step, *Experiments in Fluids*, 1987, **5**, (3), pp 154-158.

https://doi.org/10.1017/S0001924000007557 Published online by Cambridge University Press